Planetary and Space Science 66 (2012) 87–95

Contents lists available at SciVerse ScienceDirect

Planetary and Space Science

journal homepage: www.elsevier.com/locate/pss

The cratering history of asteroid (21) Lutetia

S. Marchi [a,*], M. Massironi [b], J.-B. Vincent [c], A. Morbidelli [a], S. Mottola [d], F. Marzari [e], M. Küppers [f], S. Besse [g], N. Thomas [h], C. Barbieri [i], G. Naletto [j], H. Sierks [c]

[a] Departement Cassiopée, Universite de Nice – Sophia Antipolis, Observatoire de la Côte d'Azur, CNRS, Nice, France
[b] Department of Geosciences, Padova University, Italy
[c] Max Planck Institute for Solar System Research, Lindau, Germany
[d] Institut für Planetenforschung, DLR-Berlin, Germany
[e] Department of Physics, Padova University, Italy
[f] ESA-ESAC, Villanueva de la Cañada, Madrid, Spain
[g] Laboratoire d'Astrophysique de Marseille, France
[h] Physikalisches Institut, University of Bern, Switzerland
[i] Department of Astronomy, Padova University, Italy
[j] Department of Information Engineering, Padova University, Italy

ARTICLE INFO

Article history:
Received 1 July 2011
Received in revised form
23 October 2011
Accepted 26 October 2011
Available online 7 November 2011

Keywords:
Asteroid (21) Lutetia
Asteroid cratering
Asteroid evolution
Main belt asteroids

ABSTRACT

The European Space Agency's Rosetta spacecraft passed by the main belt asteroid (21) Lutetia on 10th July 2010. With its ~100 km size, Lutetia is one of the largest asteroids ever imaged by a spacecraft. During the flyby, the on-board OSIRIS imaging system acquired spectacular images of Lutetia's northern hemisphere revealing a complex surface scarred by numerous impact craters, reaching the maximum dimension of about 55 km.

In this paper, we assess the cratering history of the asteroid. For this purpose, we apply current models describing the formation and evolution of main belt asteroids, that provide the rate and velocity distributions of impactors. These models, coupled with appropriate crater scaling laws, allow us to interpret the observed crater size-frequency distribution (SFD) and constrain the cratering history. Thanks to this approach, we derive the crater retention age of several regions on Lutetia, namely the time lapsed since their formation or global surface reset. We also investigate the influence of various factors – like Lutetia's bulk structure and crater obliteration – on the observed crater SFDs and the estimated surface ages.

From our analysis, it emerges that Lutetia underwent a complex collisional evolution, involving major local resurfacing events till recent times. The difference in crater density between the youngest and oldest recognized units implies a difference in age of more than a factor of 10. The youngest unit (Beatica) has an estimated age of tens to hundreds of Myr, while the oldest one (Achaia) formed during a period when the bombardment of asteroids was more intense than the current one, presumably around 3.6 Gyr ago or older.

1. Introduction

The European Space Agency's (ESA) Rosetta spacecraft passed by the main belt asteroid (21) Lutetia with a relative velocity of ~15 km/s on 10 July 2010 at 15:44:56 UTC. The Rosetta-Lutetia distance at closest approach (CA) was 3170 km. During the flyby the solar phase angle (sun–object–observer) decreased from the initial 11° to a minimum of 0.15° 18 minutes before CA, then increased again to 80° at CA and finally reached a maximum of 139° when the observations were stopped. A total of 400 images were obtained by the optical, spectroscopic, and infrared remote imaging system (OSIRIS), which consists of two imagers: the wide angle camera (WAC) and the narrow angle camera (NAC) (Keller et al., 2007). The best resolution at CA corresponded to a scale of 60 m/px at the asteroid surface.

Lutetia has an orbital semi-major axis of about 2.43 AU, an eccentricity of 0.16 and an inclination of 3.06°. Its shape can be fitted by an ellipsoid having axes of 121 × 101 × 75 km (Sierks et al., 2011).

Previous space missions have visited and acquired detailed data for a total of six asteroids, namely four main belt asteroids (951 Gaspra, 243 Ida, 253 Mathilde, and 2867 Steins; Veverka et al., 1999a; Belton et al., 1992, 1994; Keller et al., 2010) and two near-Earth objects (433 Eros and 25143 Itokawa; Veverka et al., 1999b;

* Corresponding author. Tel.: +33 (0)4 9200 3156.
E-mail address: marchi@oca.eu (S. Marchi).

0032-0633/$ - see front matter © 2011 Elsevier Ltd. All rights reserved.
doi:10.1016/j.pss.2011.10.010

Saito et al., 2006). Itokawa is the smallest of them, with dimensions of $0.45 \times 0.29 \times 0.21$ km. The other asteroids have average sizes ranging from ~ 5 km to ~ 53 km. In this respect, Lutetia with its average size of 98 km is the second largest asteroid ever visited by a spacecraft so far (at the moment of the writing – October 2011 – Dawn mission is orbiting around the 500-km sized asteroid (4) Vesta).

This paper analyzes some of the highest resolution OSIRIS images with the aim to study the crater size-frequency distributions (SFDs) on the different units that have been identified on the basis of geological investigations (Sierks et al., 2011; Massironi et al., 2012; Thomas et al., 2012). This analysis provides constraints on Lutetia's bulk structure and surface evolution. The observed crater SFDs are also used to compare the cratering process among the different units, to derive absolute ages and provide a chronology of the major events that affected Lutetia evolution.

2. Lutetia crater population

The NAC high resolution images acquired during the flyby were used to identify major regions on Lutetia (see Fig. 1). These regions have been defined by taking into account several factors, including local topography, geological features, surface texture, crater spatial density and stratigraphic relationships (Thomas et al., 2012; Massironi et al., 2012). In this respect, each region is characterized by distinct properties of one or more of the above listed factors. The regions identified have been further divided into several units. Thanks to this selection criterion, the defined units reflect major differences in their evolution (Massironi et al., 2012; Thomas et al., 2012). Note that the actual unit boundaries are in some cases not well established due to the lack of resolution and/or unfavorable illumination conditions (Massironi et al., 2012; Thomas et al., 2012).

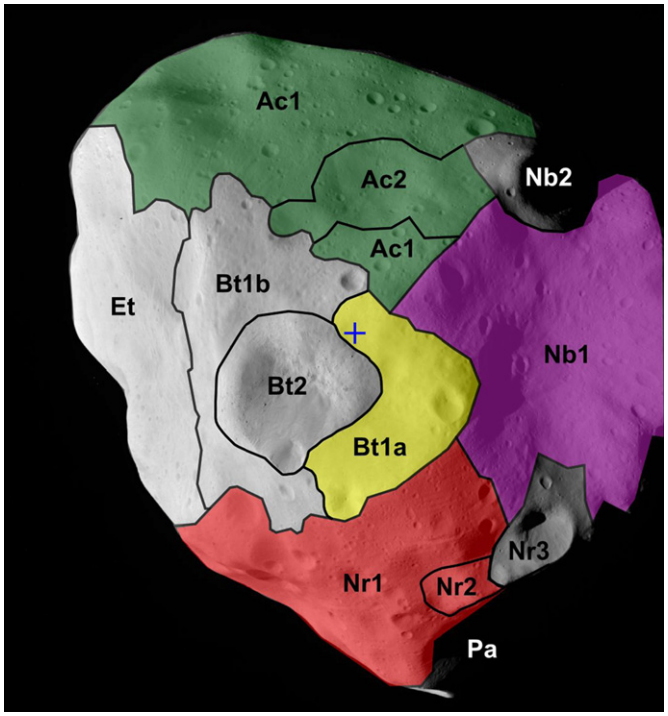

Fig. 1. The six major regions identified on Lutetia. Ac: Achaia, Nr: Noricum, Nb: Narbonensis, Bt: Baetica, Et: Etruria, Pa: Pannonia. Note that some boundaries may slightly vary according to different authors. For a more detailed definition of the regions see Massironi et al. (2012) and Thomas et al. (2012). Some of the major units (i.e., subdivisions of the regions) are also reported. Colored units are those used for crater counts. The corresponding areas (km^2) are: 760 (Bt1a), 2875 (Ac1+Ac2), 2042 (Nr1+Nr2), and 2647 (Nb1). The blue "+" at the center of the image indicates the north pole. (For interpretation of the references to color in this figure legend, the reader is referred to the web version of this article.)

Among the major regions, only four were imaged with enough quality for accurate crater counting to be performed. These are Achaia, Narbonensis, Noricum and Baetica. Their geological properties show remarkable differences, therefore they will be described individually in the following sections.

Achaia. This region is defined by a remarkably flat and uniform area. It is bounded by Baetica, Narbonensis and Etruria. Its boundaries with Baetica and Narbonensis are defined mainly by texture and topography, respectively. The boundary with Etruria is defined by the same means but, due to low contrast of the images in these regions, it is less precisely established.[1] The illumination conditions within Achaia are very good and uniform, therefore craters are clearly visible and their size estimate is performed with precision (Vincent et al., 2012).

The Achaia region (Ac1+Ac2) is heavily cratered, showing a large range of crater sizes, from 21.6 km (Nicea crater) down to the resolution limit (we used a minimum of 4 pixels to identify craters, thus about 0.2 km). The overall spatial distribution of the 157 craters >0.6 km is uniform and there appears to be no evident contamination from adjacent units (see Fig. 2, panel b). At smaller sizes, several crater-like features may not be of impact origin. Many circular depressions are close to, or overlap linear features, therefore may not represent bona fide craters. The presence of secondary craters (formed by boulders ejected during the formation of other craters) can also be possible at these small crater sizes, although it is unclear how likely can secondary craters form on Lutetia, given its low escape velocity.

For the purpose of age assessment, we are interested in primary craters (i.e., formed by impacts with asteroids), therefore our analysis focuses on craters >0.6 km. The resulting crater SFD is shown in Fig. 3 (panel a).

An interesting result is that Achaia's crater SFD exhibits a marked flexure point at about 4–7 km. Note that the observed flexure point is unlikely due to observational biases, like uncertainties in the identification of craters or resolution issues. This is because Achaia region is a remarkably flat area and it has been imaged with uniform conditions of illumination, while the flexure point is well above the image resolution. Moreover, thanks to the boundary selection, we also exclude that the observed flexure is due to obliteration of small craters due to crater ejecta coming from nearby units (e.g., Beatica). For the same reason, it seems also unlikely that the formation of the large crater Massalia (see next sections) played a role in the formation of the flexure point in Achaia crater SFD.

Noricum. This unit has a very complex topography. It contains a number of closely packed and prominent circular features, likely impact craters, showing several stages of degradation (Vincent et al., 2012). Moreover, this unit looks "compressed" among the impact craters of Baetica, Massalia crater, and possibly another large crater on the dark side of Lutetia (namely, Pannonia region; see Fig. 1), the presence of which may be inferred thanks to the circular terminator of part of Noricum. These factors are likely at the origin of Noricum complex topography.

Crater counts have been performed in unit Nr1+Nr2 (for simplicity we will refer to Noricum region in the rest of the work). The overall viewing geometry is not optimal (i.e., nearly edge-on), therefore the size estimate of some of the 76 identified

[1] Note that several choices of the Etruria–Achaia boundary have been performed in our analysis. The influence on the actual choice on the resulting Achaia crater SFD is negligible.

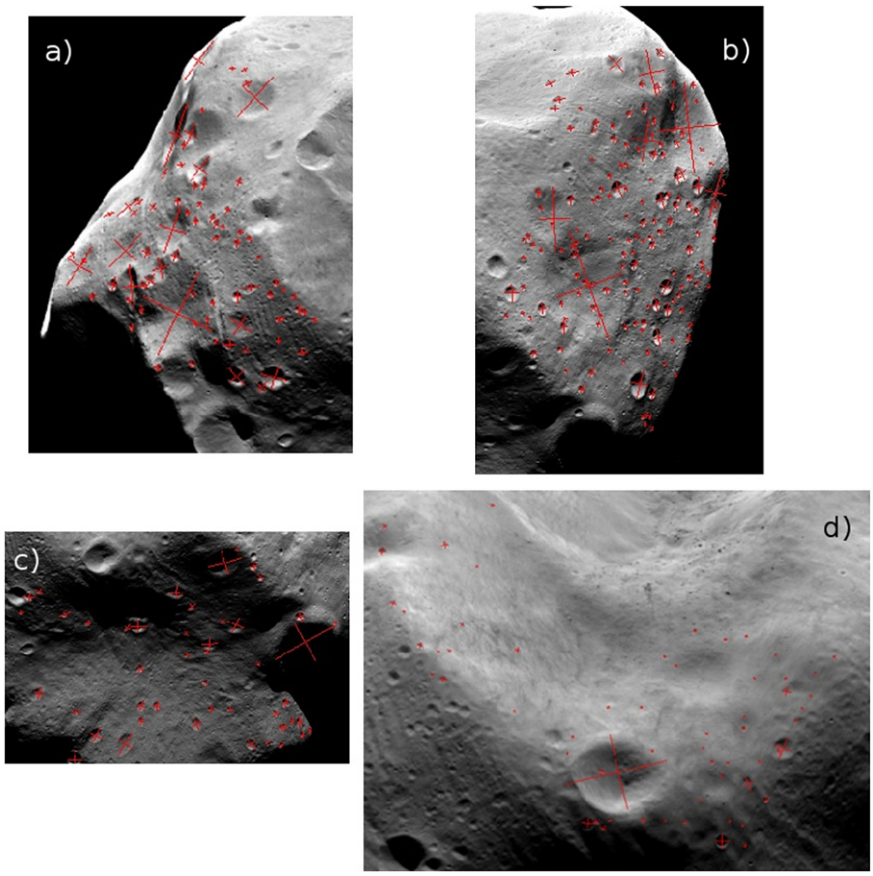

Fig. 2. The panels indicate the craters counted on the four units investigated. Crater counts have been performed on image NAC.15.42.41.240 for Achaia (b), Noricum (a) and Narbonensis (c) regions, and on image NAC.15.44.41.262 for Bt1a region (d).

craters (>0.6 km) is problematic (see Fig. 2, panel a). The resulting crater SFD shows a clear transition at about 2 km (see Fig. 3, panel b): the slope of the crater SFD for $D>2$ km is considerably shallower than that for $D<2$ km. The feature resembles somewhat the flexure seen on Achaia crater SFD, although in this case it may be due to imprecise size estimate for several large craters due to their nearly edge-on view. The crater spatial density for $D<2$ km is very similar to that of Achaia.

Narbonensis. This region corresponds to the interior of the 55-km-sized crater Massalia, the largest impact structure detected on Lutetia. Crater count has been performed in unit Nb1 (for simplicity we will refer to Narbonensis region in the rest of the work). A total of 47 craters >0.6 km have been identified (see Fig. 2, panel c). Notably, several craters appear deformed by sliding of their rims due to the relatively high topographic slope present in large part of the unit (Vincent et al., 2012, see also Fig. 4, upper panels). In these cases, the determination of the actual crater size is not very accurate.

Overall, the crater spatial density of Narbonensis is lower than that of Achaia (see Fig. 3, panel c). The shapes of the crater SFDs of the two units also differ. In particular, the Narbonensis crater SFD has a shallower slope at small sizes than Achaia. It is not clear whether this difference is due to poor count statistics or it is a real feature. In the latter case, it might be due to variation in the local properties of the terrains or due to some later modification (as we will discuss later).

Baetica. This region, unlike the previous ones, shows marked evidence of several major modification processes (landslides, ejecta blanketing, etc.) that have been used to establish sub-units that likely formed at different epochs (Thomas et al., 2012; Massironi et al., 2012). Moreover, this region is also characterized by large topographical slope variations (from 0° to 45°, see Fig. 4, lower panels), and by the presence of many large boulders (Kueppers et al., 2012).

Overall, the Baetica region presents much fewer craters than adjacent regions. Some Baetica's units appear extremely young, showing no detectable impact craters. For these reasons, we restrict our analysis to a unit, named Bt1a (see Fig. 1), which apparently has not been affected by recent geological processes (e.g., landslides), it is relatively flat and uniform, and does contain a fair number of small impact craters. In this case, we boost crater detection by using Laplacian-filtered images.[2] We identify 62 craters in the range 0.2–1 km (see Fig. 2, panel d).

The Bt1a crater SFD shows an overall shape consistent with those of other units, and it is characterized by a much lower crater spatial density (see Fig. 3, panel d). Interestingly, Bt1a contains a fresh and large (~ 7 km) crater, plus a second highly degraded crater having similar dimensions that has not been counted since it probably formed before Bt1a (Thomas et al., 2012; Vincent et al., 2012).

3. The model production function chronology

The crater SFDs of the units presented in the previous section can be used to derive their crater retention ages. The age of units is a crucial information, since it provides constraints on the formation and evolution of Lutetia. In this respect, Lutetia stands

[2] The Laplacian filter technique uses secondary derivatives in two directions to enhance the contrast of the input image and it is known to be very effective in revealing small, high frequency features (Besse et al., submitted for publication).

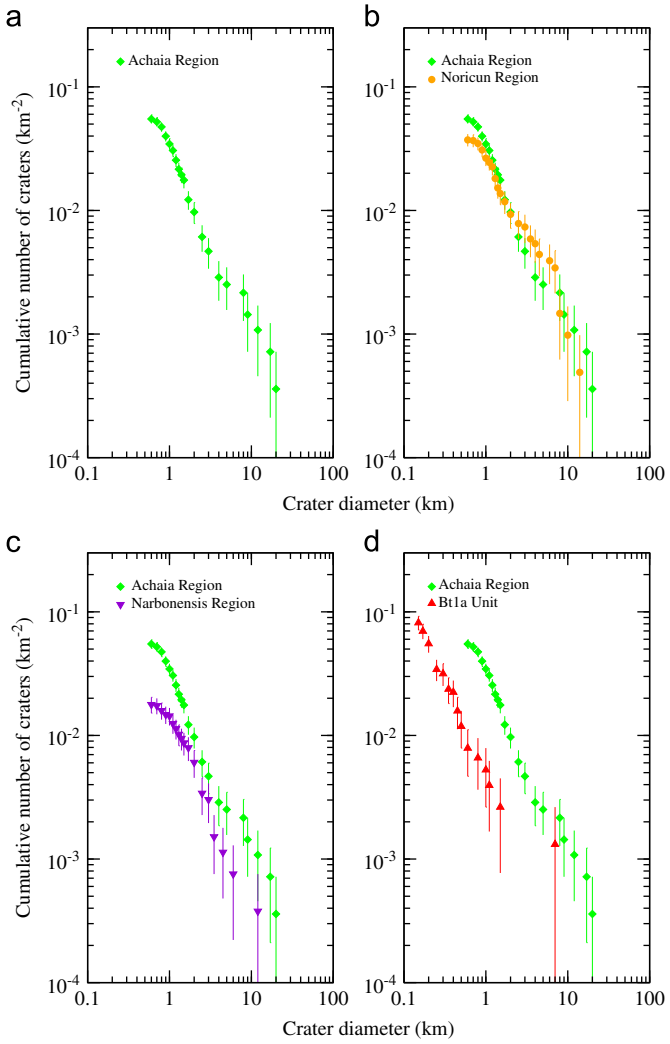

Fig. 3. Crater size-frequency distributions of the four units reported in Fig. 2 (Achaia region (a), Noricum region (b), Narbonensis region (c), and Bt1a unit (d)). Achaia crater SFD is reported in all panels for a better comparison.

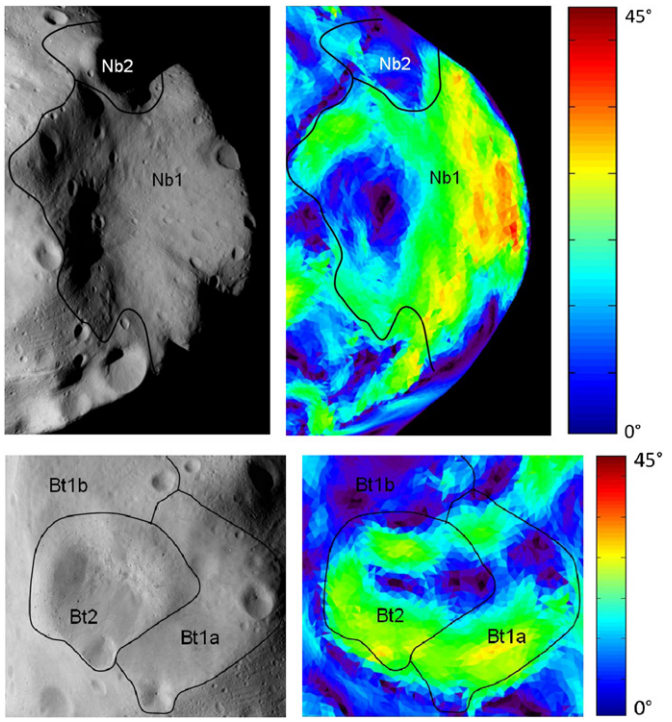

Fig. 4. Close view of Narbonensis and Baetica regions (top-left and bottom-left panels, respectively). Topographical slope (i.e., the angle between local shape and local gravity) for Narbonensis (top-right panel) and Baetica (bottom-right panel) regions.

out with respect to all previously visited asteroids (except Vesta), for its complex geological evolution. Therefore, the crater retention ages of its units are important to set a timeline for this evolution. Moreover, the study of the cratering process along with geological assessment can be used to constrain the physical properties of the target.

In this work, crater retention ages are derived in the framework of the model production function (MPF) chronology (Marchi et al., 2009). With this approach Lutetia's crater production function (i.e., the expected number of craters per year per unit surface) is computed by modeling its impactor flux and by using a crater scaling law in order to compute the resulting crater population. The resulting crater MPF gives the cumulative density of craters (per year) as a function of the crater size.

In analogy with previous work, the impactor flux is characterized by its size-frequency distribution and impact velocity distribution. The impactor SFD is taken from the model population of main belt asteroids of Bottke et al. (2005). In this work, we will also consider a second MBA population derived by the sub-kilometer asteroid diameter survey (SKADS) (Gladman et al., 2009, see Fig. 5). Using the Farinella and Davis (1992) algorithm, we computed that the intrinsic collision probability between MBAs and Lutetia is $P_i = 4.21 \times 10^{-18}$ km^{-2} yr^{-1}. Note that this P_i value is significantly higher that the average value for the main belt, namely 2.86×10^{-18} km^{-2} yr^{-1}. Using the same algorithm, we also computed Lutetia's impact velocity distribution (see Fig. 6).

Concerning the crater scaling law, we adopted a Pi-group scaling law (Holsapple and Housen, 2007). These scaling laws allow us to estimate the size of a crater given the dimension (d) and velocity (v) and density (δ) of the impactor along with the density (ρ) and strength (Y) of the target. In addition to these quantities, two parameters (ν,μ) account for the nature of the terrains (hard rock, cohesive soil, and porous material). In this paper, we investigate both hard rock and cohesive soils scaling laws, whose parameters are $\nu = 0.4$, $\mu = 0.55$ and $\nu = 0.4$, $\mu = 0.41$, respectively. We assume $Y = 2 \times 10^8$ dyne/cm^2 for typical hard rock and an impactor density of $\delta = 2.6$ g/cm^3 (Marchi et al., 2010). The bulk density of Lutetia is $\rho = 3.4$ g/cm^3 (Sierks et al., 2011). Values of density and strength for cohesive soils will be given in Section 4. Further details about the crater scaling law can be found in Marchi et al. (2011). Note that no correction for the transient-to-final crater size has been applied, because the crater modification stage is not likely to occur on Lutetia given its low gravity.

Absolute ages can be computed by knowing the time dependence of the impactor flux in the past. Unfortunately, such time-dependence is not known for main belt asteroids. Two approaches can be used to overcome such a limitation. First, one can assume that the present impact rate for main belt asteroids remained constant over the age of the solar system. This scenario requires a constant main belt population, where no big modification (e.g., in its orbital architecture and total mass) occurred. However, it is known that the main belt was more massive in the past and that during the early phases of the solar system it was shaped by major events (e.g., Morbidelli et al., 2010). However, these processes have not yet been modeled with enough certainty and accuracy to enable the determination of the time evolution of the impact rate. An alternative approach is to refer to the lunar impactor flux, which has been calibrated on the basis of radiometric ages of lunar

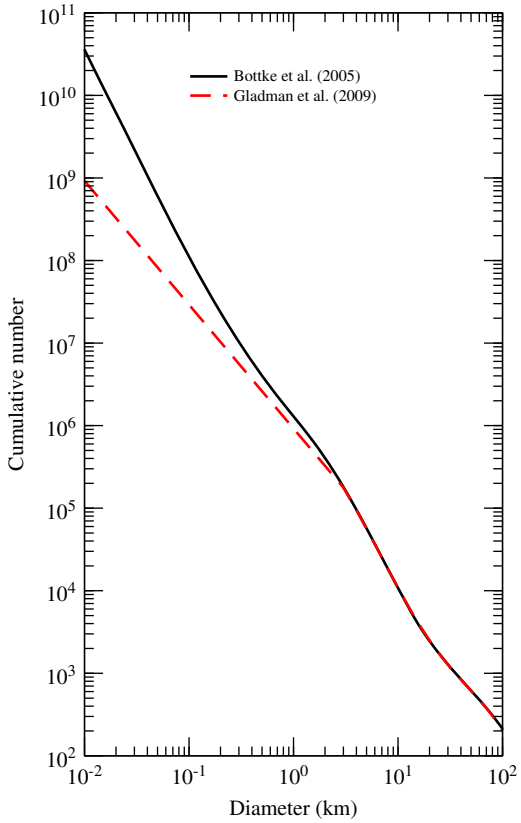

Fig. 5. Main belt size-frequency distributions used in this work. The model Bottke et al. (2005) distribution is based on the observed debiased main belt population down to about 1 km. The Gladman et al. (2009) distribution is obtained in the following manner: for impactor sizes $\gtrsim 3$ km (corresponding to the completeness limit of H-magnitude ~ 15, for an assumed albedo of 0.2), it overlaps with the Bottke et al. (2005) SFD; while for sizes <3 km it is has a cumulative slope of -1.5. Note that the SKADS survey is valid down to $H \sim 18$ (corresponding to about 0.8 km), nevertheless we extrapolated the -1.5 slope to smaller sizes.

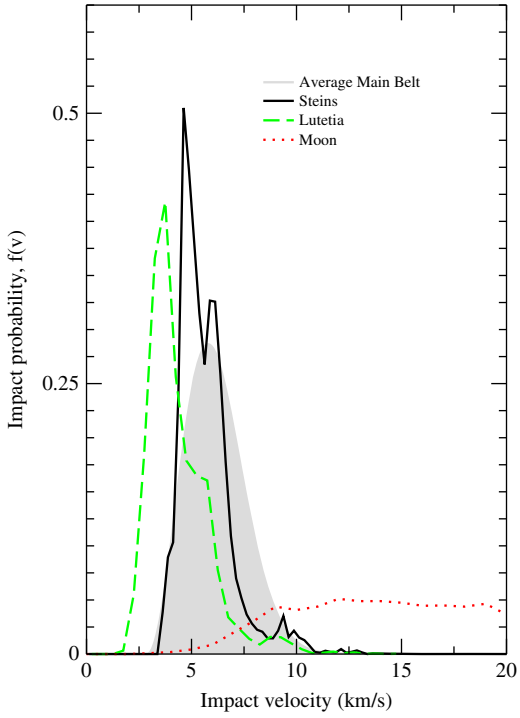

Fig. 6. Lutetia's impact velocity distribution. For a comparison, the distribution for Steins, the average main belt (shaded area) and the Moon (largely out of scale) are also reported. The average impact velocity for Lutetia is 4.3 km/s.

samples (Neukum and Ivanov, 1994; Marchi et al., 2009). This scenario assumes that the impactor flux variation experienced by the Moon also applies to main belt asteroids. In reality, since the Moon is not embedded in the main belt, it is likely that the Moon and MBAs had very different impact histories. For instance, consider the case that the lunar impact cataclysm between 4.1 and 3.8 Gy ago was due to a temporary destabilization of the main belt that removed a part of its asteroids. Then the Moon would have suffered an impact spike, while the impact rate in the asteroid belt would have decreased (i.e., without impact spike) from an initial higher but roughly constant value in the 4.5−4.1 Ga time-interval, to the current value. Thus, the time evolutions of the impact rate on the Moon and in the asteroid belt would have been totally different. On the other hand, in the case of a large cometary contribution to the lunar cataclysm (i.e., from a source region outside the main belt) these bodies would have produced an impact spike on both the Moon and MBAs.

In the assumption that the evolution of the impact rate in the asteroid belt and on the Moon was the same, and assuming that all craters that are formed are retained on the surface, the crater MPF function for an asteroid at a time t is given by

$$\mathrm{MPF}(D,t) = \mathrm{MPF}(D,1\ \mathrm{yr}) \cdot \frac{N_1(t)}{N_1(1\ \mathrm{yr})} \quad (1)$$

where D is the crater size and $N_1(t)$ expresses the lunar crater cumulative number at 1 km as a function of time according to the following equation:

$$N_1(t) = a(e^{bt}-1)+ct \quad (2)$$

where t is in Gyr ($t=0$ is the present time), $a=1.23\times10^{-15}$, $b=7.85$, $c=1.30\times10^{-3}$ (Marchi et al., 2009).[3] Note that setting $a=0$ would correspond to the constant flux scenario. The MPF(D,t) is used to derive the model cratering age by a best fit of the observed crater SFD that minimizes the reduced chi squared value, χ_r^2. Data points are weighted according to their measurement errors. The formal errors on the best age correspond to a 50% increase of the χ_r^2 around the minimum value. Other sources of uncertainties are neglected (see Marchi et al., 2011, for more details).

Eq. (1) basically implies that MPF(D,t) is obtained by simply y-axis shifting MPF(D,1 yr) by a proper amount. It has been shown by previous studies on asteroid cratering, however, that several crater obliteration processes may be at work (e.g., O'Brien et al., 2006). In the case that crater obliteration occurs, the shape of the MPF changes over time and may reach a steady-state in the case that crater saturation occurs (namely, the newly formed craters erase previous ones leaving the overall crater spatial density unchanged). In this paper, we take into account crater obliteration processes as described in Marchi et al. (2010).

4. Crater retention age estimates

One important aspect of MPF methodology is that it depends on the assumed properties of the target body (Massironi et al., 2009; Marchi et al., 2011). Therefore, the analysis of crater SFDs on

[3] The parameters a,b,c for the lunar chronology curve are determined by best fit of lunar calibration data and their actual values may vary according to different authors (e.g., Neukum and Ivanov, 1994). However, the variation of the actual values for a,b,c has a negligible impact on the age determination.

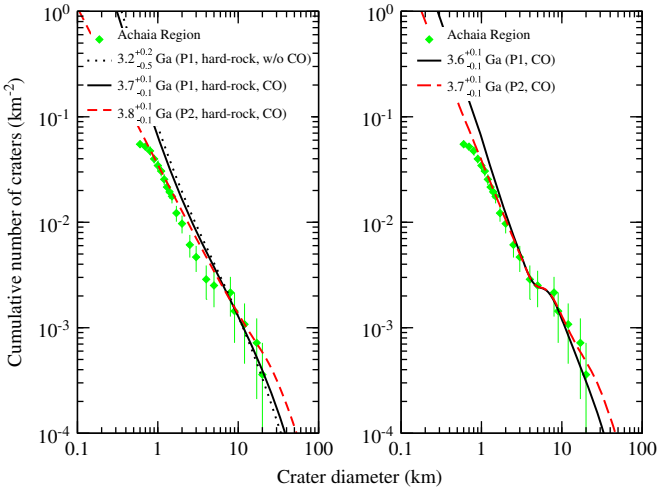

Fig. 7. Achaia MPF best fit. Left panel: Best fits obtained using hard rock scaling law, with and without crater obliteration (CO), and using the MBA population from Bottke et al. (2005) (P1) and Gladman et al. (2009) (P2). Right panel: Best fits obtained modeling a transition in the physical properties of Achaia region, namely adopting a fractured layer onto a more competent interior (see text for more details).

different terrains on the same body (or different asteroids) should be done with caution, since changes in the material properties may invalidate direct comparison (Marchi et al., 2011). Generally speaking, material properties are not known in detail, however, in some cases, they can be constrained on the basis of geomorphological and geological analysis. Therefore, whenever possible, MPF chronology allows to derive cratering ages taking into account explicitly the effect of the inferred material properties. In this section we present the results of our MPF-based age estimate for each unit investigated.

Achaia. As described in the previous section, Achaia crater SFD is characterized by a flexure point located at $4 < D < 7$ km. Fig. 7 reports the results of MPF best fitting of the observed crater SFD. The left panel shows the best fits obtained by using Bottke et al. (2005) population (P1 hereinafter) and the crater scaling law for hard rock both with and without crater obliteration. Concerning the crater obliteration process, we took into account local regolith jolting and crater superposition and adopted the same parameters used by O'Brien et al. (2006). Global seismic effects and cumulative seismic shaking have not been considered because of the large size of Lutetia.[4] The present fits are achieved anchoring the MPF to the large crater end of the crater SFD. The quality of the fit is basically the same in the two scenarios, except for a slightly older age in case of crater obliteration. These results clearly show that P1 is not able to accurately reproduce the observed cratering. A similar conclusion is reached also using the Gladman et al. (2009) population (P2 hereinafter). In particular, the observed flexure in the crater SFD has no correspondence in either MBA populations. Indeed, the impactor population is not known at the impactor size relevant for the flexure ($\sim 0.5-0.8$ km) and therefore it is possible that the real main belt SFD may account for it. Nevertheless, the fact that such a feature has not been observed on other large asteroids, like Ida and Mathilde (Sierks et al., 2011), makes this unlikely.

We have excluded that the flexure is due to the impactor flux, global and local obliteration processes, and observational biases (see also discussion in Section 2). A further possibility is that the flexure is related to terrain properties. As shown for Mercury (Marchi et al., 2011), the presence of a stratified target having fractured material at the surface overlying a more competent interior would produce a crater SFD showing a characteristic flexure. Such a flexure is the combined result of (i) adopting different material parameters for the fractured layer and the competent interior and (ii) using cohesive soil and hard rock scaling laws for the two layers (Marchi et al., 2011). The position of the flexure is mainly determined by the thickness of the fractured material, which can be chosen in order to produce a best fit of the observed crater SFD. We investigated this possibility, by modeling a transition in the Achaia properties, as done in Marchi et al. (2011). The results are shown in Fig. 7 (right panel). The P1 best fit is now improved, being in overall good agreement with the crater SFD. The resulting age is 3.6 ± 0.1 Ga, obtained for a fractured layer depth of 3 km. It must be clear that the above age derives from the lunar chronology (Eq. (1)), whose applicability to main belt asteroids is unclear. It is also noteworthy that extrapolating the present main belt impact rate in the past would lead to an age older than that of the solar system. This suggests that the main belt experienced a heavy bombardment in the past, although not necessarily with the time-dependence described by Eq. (1). The use of the lunar chronology probably provides a lower bound to the real age, whereas the age computed assuming a constant flux provides an upper bound (in this case a trivial one).

The best fit presented in Fig. 7 shows a residual mismatch for craters 0.6–2 km (much above resolution limit), the origin of which is unclear. Here we show that, using a shallower MBA population – such as P2 – would produce a better match of the observed crater SFD. The resulting age is 3.7 ± 0.1 Ga. Note, however, even in the presence of a shallower population a stratified target is needed in order to explain the flexure (Fig. 7, left panel). It must be clear that the SKAD survey is valid down to an absolute magnitude of ~ 18 (corresponding to a size of 0.8 km for a geometric albedo of 0.15). Such impactors would produce crater sizes of the order of several km, therefore in our fit we extrapolated P2 slope outside its range of validity.

We also find that, independently of the MBA population used, the Achaia crater SFD is not saturated. Indeed, at least with the crater obliteration parameters adopted here, the saturation occurs at a higher crater density than observed on Achaia. However, we caution that this conclusion depends on the not-well-known process of crater obliteration. A more thorough analysis of this issue is deferred to future work.

Baetica. This unit is characterized by the presence of a widespread regolith layer. The thickness of this layer is unknown, although both crater and landslide morphologies have been used to constrain its depth to be at least hundreds of meters (Vincent et al., 2012). Therefore, it seems likely that all the craters (except maybe for the few largest ones) detected in Bt1a formed in highly granular, cohesive soils. As for the strength, reference values are from the lunar regolith ($Y \sim 3 \times 10^4$ at a depth of 3 m) and terrestrial alluvium ($Y \sim 7 \times 10^5$). Here, we investigate strength values ranging from 10^5 to 10^7 dyne/cm^2. We also take a density of 2 g/cm^3, typical of lunar regolith.

The resulting MPF best fit, using P1 population, is shown in Fig. 8. The main conclusion is that Bt1a is very young, ranging from ~ 4 to ~ 50 Ma, according to the value of the strength used. The same figure also shows the best fit achieved with P2. The quality of the fit is now much improved, given the SKADS' shallower SFD slope. In this case the derived ages range from ~ 50 to ~ 220 Ma. Note that the last age is in better agreement with the boulder lifetime estimated for the central (and youngest) unit of Baetica (Kueppers et al., 2012).

The overall wavy shape of the observed crater SFD is not accurately reproduced by the MPFs. This may have several

[4] To see this, we rescaled Ida's global erasing curve from Figure 4 of O'Brien et al. (2006) to Lutetia. It results that a crater of about 100 km would be needed to globally erase craters ≥ 1 km. This result also suggests that it is unlikely that the formation of Massalia crater triggered global surface reset.

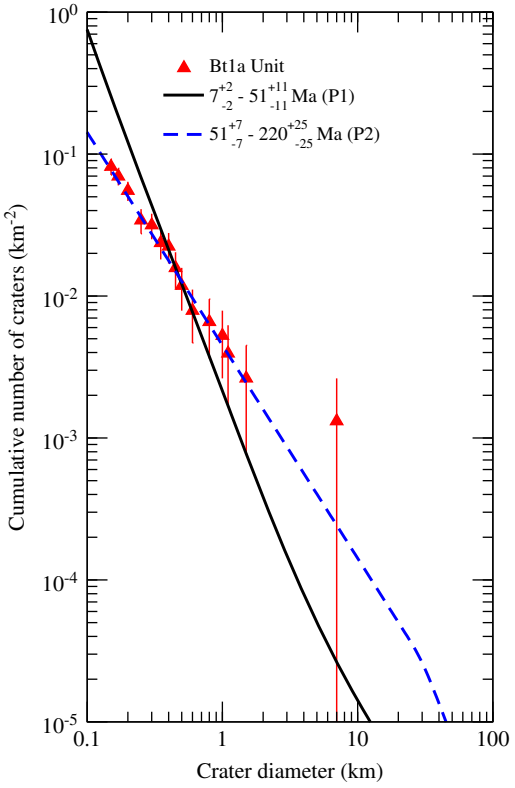

Fig. 8. Baetica MPF best fit for two impactor populations. The crater scaling law for cohesive soil has been used. The derived age ranges correspond to two limiting values of strength, namely 10^5 and 10^7 dyne/cm^2, respectively. No crater obliteration has been applied here, given the very young ages involved (see text for further details).

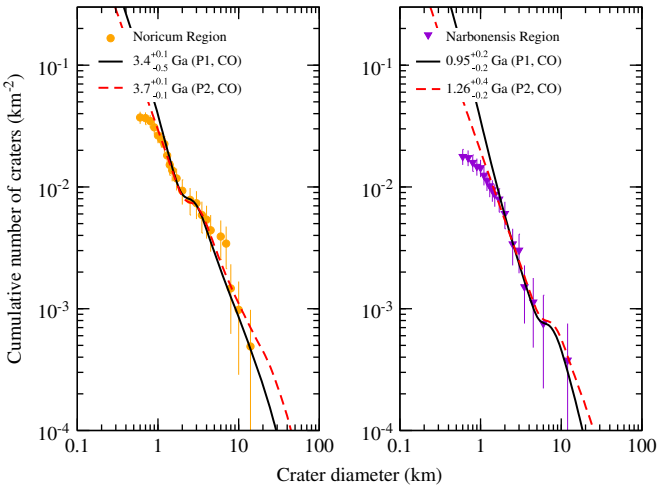

Fig. 9. Noricum and Narbonensis MPF best fits (see text for further details).

explanations, including low crater statistics and a poor knowledge of the MBA SFD at these small sizes. Note that it is also possible, given the large topographical slopes present in this area, that small craters are not well preserved (see Fig. 4, lower panels).

Noricum and Narbonensis. These two units present several difficulties in their age assessment. Both crater SFDs are not well fit by the MPFs, possibly because of errors in the crater size measurements (Noricum) and poor statistics (Narbonensis). Some constraints on the expected evolution of these units come for geological analysis. First of all, it is clear from stratigraphical arguments that Massalia crater formed later in time with respect to both Achaia and Noricum (Massironi et al., 2012). Therefore, the Narbonensis unit is younger than Achaia and Noricum. Moreover, in the light of the arguments discussed in previous sections, it appears difficult that the formation of Massalia globally reset Lutetia's surface. This conclusion is also in agreement with hydrocode simulations of Massalia formation. Note that these simulations (Cremonese et al., 2012) predict that the Massialia event triggered the formation of a fractured layer generated all over the surface of Lutetia. The actual damage of the fractured layer depends on the resolution of the simulations, nevertheless it is believed to be not sufficient to cause global resurfacing (K. Wünnemann, pers. comm. on 27 June 2011).[5]

If the above scenario is correct, then we expect that Noricum has similar properties as Achaia. Fig. 9 (left panel) shows the MPF best fit using a stratified target model and crater obliteration. The best fit is achieved with a fractured layer depth of 1.3 km. The resulting Noricum age is ~3.4 and ~3.7 Ga for P1 and P2, respectively, which is consistent with being coeval with Achaia (again, we point out that these ages are derived using the lunar chronology). The relatively shallow layer of fractured material may also be consistent with the complex topography of the units (possibly reflecting a more competent near-surface interior).

Fig. 9 (right panel) shows the MPF best fit of Narbonensis. In this case, the observed crater SFD does not show evidences of a flexure, possibly due to the poor crater statistics, that would suggest the presence of stratified terrains. Nevertheless, according to Cremonese et al. (2012), the interior of the Massalia crater is expected to be fractured up to the depth of several km. Therefore, by using the same crater scaling law and a fractured layer depth of 3.5 km (although larger depths are also possible), we obtain a best-fit age of ~0.95 and ~1.3 Ga for population P1 and P2, respectively.

This latter result is puzzling, since such a large crater is not expected to be so young. Note that the inferred age is quite insensitive to the adopted scaling law or impactor population. We estimated that the impactor that formed Massalia was in the size range 7–9 km (Sierks et al., 2011). The current frequency of such impacts is about one every 9 Ga. The computed a priori probability that such an event happened in the last 1 Ga, is ~11%. On the other hand, knowing that the Massalia event did happen within the last 4.5 Ga, the probability that such event occurred in the last 1 Ga, is ~25%. These numbers apply for the present main belt impact rate, and thus certainly represent an upper limit because it is believed that the impact rate in the primordial main belt was at least a factor ~2–4 more intense than today (Morbidelli et al., 2010). This would imply that Massalia event more likely happened early on rather than recently. Thus, in conclusion, it is likely that other processes may be responsible for a lack of craters within Narbonensis (Massironi et al., 2012; Thomas et al., 2012).

As discussed in the previous section, this unit has relatively high topographical slopes and episodes of slopes slumping may have induced crater erasing (see Fig. 4, upper panels). The presence of significant rims slumping is supported by the V-shaped topographical profile of the crater (Preusker et al., 2012). Comparing the observed profile with a typical profile of a fresh crater (Cremonese et al., 2012), we derive that several hundred meters of rim material may have been displaced toward the center of the crater, which may be enough to explain the relatively young age of this unit.

[5] We also acknowledge the fact that these conclusions are based on scaling laws and simulations which depend on poorly constrained parameters. Thus, it is possible – although unlikely – that the formation of Massalia crater triggered major crater reset on nearby regions.

5. Discussions and conclusions

The main result of our crater retention age analysis is that it confirms a prolonged and complex collisional evolution of Lutetia. As shown for previous asteroids visited by spacecraft, collisions play a major role in the evolution of any asteroid, being largely responsible of their shapes, internal structure and geomorpohological features. The latter play also an important role for the understanding of surface spectrophotometric properties.

All these collisional-related processes are well documented on Lutetia, and can be used to constrain its evolution. The derived ages of the main units of Lutetia show its active collisional history, lasting for about 4 Ga. The extremely young Bt1a unit, with an age of <220 Ma, indicates that major (collisional) events occurred until very recent times. We also find evidence on the oldest Achaia region – and possibly Noricum region – of a non-uniform radial strength profile, possibly due to the effects of previous collisions that produced a highly fractured surface on top a competent interior. In this respect, Lutetia resembles what has been found on other much larger bodies like Mercury and the Moon (Marchi et al., 2011). It is also noteworthy that the observed cratering seems to be produced by a population having a shallower cumulative slope than predicted by the Bottke et al. (2005) model. The overall slope seems to be consistent with recent observations (Gladman et al., 2009), although our size range of interest extends beyond their observational limits. This result, if confirmed by further studies, will require a revision of the present collisional models.

On the other hand, according to the present theories of main belt evolution, Lutetia should be a primordial object (Bottke et al., 2005). This is also confirmed by Lutetia's high density that makes it unlikely to be a fragment of a larger body (Weiss et al., 2012). This consideration is, however, in contradiction with the derived crater retention ages. Either the chronology scheme is not accurate, or some major event occurred in Lutetia history to reset its surface.

Concerning the adopted lunar chronology, it likely underestimates the real ages of main belt asteroids. Indeed, the exponential increase of the lunar impactor flux for ages older than 3.5 Ga did not likely take place in the main belt unless the main belt suffered an intense cometary bombardment. In fact, in the current scenario of main belt evolution during the Late Heavy Bombardment (LHB) at ~ 3.9 Ga, the main belt depleted by a factor of 2–4 at most (Morbidelli et al., 2010). On the other hand, the lunar chronology (Eq. (2)) predicts an increase in the impactor flux of about a factor of ~ 5 and ~ 40 in the time spans 3.5–3.9 Ga and 3.5–4.2 Ga, respectively. This steep increase in the impactor flux results in too young crater retention ages of asteroid surfaces. However, dynamical models of the early evolution of the main belt are not yet robust enough to be used successfully for precise age determination.

Concerning possible resetting event(s), the most energetic event that we can infer is the formation of Massalia crater, which, according to the previous discussion, was not able to reset the whole surface. Unless this conclusion is affected by poorly constrained parameters or other more energetic event(s) took place in the Lutetia southern hemisphere (not imaged by OSIRIS), this option appears untenable.

Lutetia's crater age conundrum still remains unsolved. Nevertheless, we expect major improvements in our theoretical and observational understandings of the main belt in the near future. In particular, the Dawn mission arrived at Vesta, the second largest asteroid, in July 2011. High resolution imaging of Vesta will help to constrain the early impact history of the main belt and the evolution of its primordial asteroids, Lutetia included.

Acknowledgments

We thank the referee D. O'Brien and an anonymous referee for helpful comments which improved the manuscript.

OSIRIS was built by a consortium of the Max-Planck-Institut für Sonnensystemforschung, Katlenburg-Lindau, Germany, CISAS – University of Padova, Italy, the Laboratoire d'Astrophysique de Marseille, France, the Instituto de Astrof A sica de Andalucia, CSIC, Granada, Spain, the Research and Scientific Support Department of the European Space Agency, Noordwijk, The Netherlands, the Instituto Nacional de Tecnica Aeroespacial, Madrid, Spain, the Universidad Politechnica de Madrid, Spain, the Department of Physics and Astronomy of Uppsala University, Sweden, and the Institut für Datentechnik und Kommunikationsnetze der Technischen Universität Braunschweig, Germany. The support of the national funding agencies of Germany (DLR), France (CNES), Italy (ASI), Spain (MEC), Sweden (SNSB), and the ESA Technical Directorate is gratefully acknowledged.

We thank the Rosetta Science Operations Centre and the Rosetta Mission Operations Centre for the successful flyby of (21) Lutetia.

References

Belton, M.J.S., Chapman, C.R., Veverka, J., Klaasen, K.P., Harch, A., Greeley, R., Greenberg, R., Head III, J.W., McEwen, A., Morrison, D., Thomas, P.C., Davies, M.E., Carr, M.H., Neukum, G., Fanale, F.P., Davis, D.R., Anger, C., Gierasch, P.J., Ingersoll, A.P., Pilcher, C.B., 1994. First images of asteroid 243 Ida. Science 265 (September), 1543–1547.

Belton, M.J.S., Veverka, J., Thomas, P., Helfenstein, P., Simonelli, D., Chapman, C., Davies, M.E., Greeley, R., Greenberg, R., Head, J., 1992. Galileo encounter with 951 Gaspra—first pictures of an asteroid. Science 257 (September), 1647–1652.

Besse, S., et al. Identification and physical properties of craters on asteroid (2867) steins. Icarus, submitted for publication.

Bottke, W.F., Durda, D.D., Nesvorný, D., Jedicke, R., Morbidelli, A., Vokrouhlický, D., Levison, H.F., 2005. Linking the collisional history of the main asteroid belt to its dynamical excitation and depletion. Icarus 179 (December), 63–94.

Cremonese, G., et al., 2012. Hydrocode simulations of the largest crater on the asteroid Lutetia. Planetary and Space Science 66, 147–154.

Farinella, P., Davis, D.R., 1992. Collision rates and impact velocities in the main asteroid belt. Icarus 97, 111.

Gladman, B.J., et al., 2009. On the asteroid belt's orbital and size distribution. Icarus 202, 104.

Holsapple, K.A., Housen, K.R., 2007. A crater and its ejecta: an interpretation of deep impact. Icarus 187 (March), 345–356.

Keller, H.U., et al., 2010. E-type asteroid (2867) steins as imaged by OSIRIS on Board Rosetta. Science 327, 190.

Keller, H.U., Barbieri, C., Lamy, P., Rickman, H., Rodrigo, R., Wenzel, K., Sierks, H., A'Hearn, M.F., Angrilli, F., Angulo, M., Bailey, M.E., Barthol, P., Barucci, M.A., Bertaux, J., Bianchini, G., Boit, J., Brown, V., Burns, J.A., Büttner, I., Castro, J.M., Cremonese, G., Curdt, W., da Deppo, V., Debei, S., de Cecco, M., Dohlen, K., Fornasier, S., Fulle, M., Germerott, D., Gliem, F., Guizzo, G.P., Hviid, S.F., Ip, W., Jorda, L., Koschny, D., Kramm, J.R., Kührt, E., Küppers, M., Lara, L.M., Llebaria, A., López, A., López-Jimenez, A., López-Moreno, J., Meller, R., Michalik, H., Michelena, M.D., Müller, R., Naletto, G., Origné, A., Parzianello, G., Pertile, M., Quintana, C., Ragazzoni, R., Ramous, P., Reiche, K., Reina, M., Rodríguez, J., Rousset, G., Sabau, L., Sanz, A., Sivan, J., Stöckner, K., Tabero, J., Telljohann, U., Thomas, N., Timon, V., Tomasch, G., Wittrock, T., Zaccariotto, M., 2007. OSIRIS the scientific camera system Onboard Rosetta. Space Science Reviews 128 (February), 433–506.

Kueppers, M., et al., 2012. Boulders on Lutetia. Planetary and Space Science 66, 71–78.

Marchi, S., Mottola, S., Cremonese, G., Massironi, M., Martellato, E., 2009. A new chronology for the Moon and Mercury. Astronomical Journal 137 (June), 4936–4948.

Marchi, S., et al., 2010. The cratering history of asteroid (2867) steins. Planetary and Space Science 58, 1116.

Marchi, S., Massironi, M., Cremonese, G., Martellato, E., Giacomini, L., Prockter, L., 2011. arXiv:1105.5272. The effects of the target material properties and layering on the crater chronology: the case of Raditladi and Rachmaninoff basins on Mercury.

Massironi, M., Cremonese, G., Marchi, S., et al., 2009. Mercury's geochronology revised by applying Model Production Function to Mariner 10 data: geological implications. Geophysical Research Letters 362, 21204.

Massironi, M., et al., 2012. Geological map and stratigraphy of asteroid 21 Lutetia. Planetary and Space Science 66, 125–136.

Morbidelli, A., Brasser, R., Gomes, R., Levison, H.F., Tsiganis, K., 2010. Evidence from the asteroid belt for a violent past evolution of Jupiter's orbit. Astronomical Journal 140, 1391–1401.

Neukum, G., Ivanov, B.A., 1994. Hazards Due to Comets and Asteroids, p. 359.

O'Brien, D.P., Greenberg, R., Richardson, J.E., 2006. Craters on asteroids: reconciling diverse impact records with a common impacting population. Icarus 183 (July), 79–92.

Preusker, M., et al., 2012. The northern hemisphere of asteroid (21) Lutetia—topography and orthoimages from Rosetta OSIRIS NAC Image Data. Planetary and Space Science 66, 54–63.

Saito, J., Miyamoto, H., Nakamura, R., Ishiguro, M., Michikami, T., Nakamura, A.M., Demura, H., Sasaki, S., Hirata, N., Honda, C., Yamamoto, A., Yokota, Y., Fuse, T., Yoshida, F., Tholen, D.J., Gaskell, R.W., Hashimoto, T., Kubota, T., Higuchi, Y., Nakamura, T., Smith, P., Hiraoka, K., Honda, T., Kobayashi, S., Furuya, M., Matsumoto, N., Nemoto, E., Yukishita, A., Kitazato, K., Dermawan, B., Sogame, A., Terazono, J., Shinohara, C., Akiyama, H., 2006. Detailed images of asteroid 25143 Itokawa from Hayabusa. Science 312 (June), 1341–1344.

Sierks, H., Lamy, P., Barbieri, C., et al., 2011. Images of asteroid 21 Lutetia: a remnant planetesimal from the early solar system. Science 334, 487.

Thomas, N., et al., 2012. The geomorphology of (21) Lutetia: results from the OSIRIS imaging system onboard ESA's Rosetta spacecraft. Planetary and Space Science 66, 96–124.

Veverka, J., Thomas, P., Harch, A., Clark, B., Bell, J.F., Carcich, B., Joseph, J., Murchie, S., Izenberg, N., Chapman, C., Merline, W., Malin, M., McFadden, L., Robinson, M., 1999a. NEAR encounter with asteroid 253 mathilde: overview. Icarus 140 (July), 3–16.

Veverka, J., Thomas, P.C., Bell III, J.F., Bell, M., Carcich, B., Clark, B., Harch, A., Joseph, J., Martin, P., Robinson, M., Murchie, S., Izenberg, N., Hawkins, E., Warren, J., Farquhar, R., Cheng, A., Dunham, D., Chapman, C., Merline, W.J., McFadden, L., Wellnitz, D., Malin, M., Owen Jr., W.M., Miller, J.K., Williams, B.G., Yeomans, D.K., 1999b. Imaging of asteroid 433 Eros during NEAR's flyby reconnaissance. Science 285 (July), 562–564.

Vincent, J.B., et al., 2012. Physical properties of craters on asteroid (21) Lutetia. Planetary and Space Science 66, 79–86.

Weiss, B., et al., 2012. Possible evidence for partial differentiation of asteroid Lutetia from Rosetta. Planetary and Space Science 66, 137–146.